

01010  
00101001  
10101001  
01010101  
110101001  
10101001  
00101010  
010101001  
110101010  
11010101001  
1010101010  
11010101001

# COMPUTATIONAL AND STRUCTURAL BIOTECHNOLOGY JOURNAL

journal homepage: [www.elsevier.com/locate/csbj](http://www.elsevier.com/locate/csbj)



## Mini Review

# Structural Consideration of the Working Mechanism of Fold Type I Transaminases From Eubacteria: Overt and Covert Movement

Sunghark Kwon, Hyun Ho Park \*

College of Pharmacy, Chung-Ang University, Dongjak-gu, Seoul 06974, Republic of Korea

## ARTICLE INFO

### Article history:

Received 12 April 2019

Received in revised form 12 July 2019

Accepted 19 July 2019

Available online 23 July 2019

### Keywords:

Transaminase

Pyridoxal 5'-phosphate

Dual substrate specificity

Conformational change

Transamination

## ABSTRACT

Transaminases (TAs) reversibly catalyze the transfer reaction of an amino group between an amino group donor and an amino group acceptor, using pyridoxal 5'-phosphate (PLP) as a cofactor. TAs are categorized according to the amino group position of the donor substrate and respective TAs recognize their own specific substrates. Over the past decade, a number of TA structures have been determined by X-ray crystallography. On the basis of the structural information, the detailed mechanism of substrate recognition by TAs has also been elucidated. In this review, fold type I TAs are addressed intensively. Comparative studies on structural differences between the apo and holo forms of fold type I TAs have demonstrated that regions containing the active site exhibit structural plasticity in the apo form, facilitating PLP insertion into the active site. In addition, given that TAs recognize two different kinds of substrates, they possess dual substrate specificity. It is known that spatial rearrangements of active site residues occur upon binding of the substrates. Intriguingly, positively charged residues are predominantly distributed at the active site cavity. The electric field generated by such charge distributions may attract negatively charged molecules, such as PLP and amino group acceptors, into the active site. Indeed, TAs show remarkable dynamics in diverse aspects. In this review, we describe the comprehensive working mechanism of fold type I TAs, with a focus on conformational changes.

© 2019 The Authors. Published by Elsevier B.V. on behalf of Research Network of Computational and Structural Biotechnology. This is an open access article under the CC BY-NC-ND license (<http://creativecommons.org/licenses/by-nc-nd/4.0/>).

## Contents

1. Introduction . . . . .	1031
2. Architecture of TAs . . . . .	1032
2.1. Typical Overall Structure . . . . .	1032
2.2. Active Site Chemistry . . . . .	1032
2.3. Multimeric State as a Functional Unit . . . . .	1034
3. Structural Differences Between the Apo and Holo Forms . . . . .	1034
4. Dual Substrate Recognition Mechanism . . . . .	1036
5. Electrostatic Steering for Cofactor and Substrate Binding . . . . .	1036
6. A Possible Working Mechanism of TAs . . . . .	1037
7. Summary and Outlook . . . . .	1037
Funding Source . . . . .	1038
Acknowledgements . . . . .	1038
References . . . . .	1038

**Abbreviations:** Cv- $\omega$ TA, *Chromobacterium violaceum*  $\omega$ -transaminase; Ms- $\beta$ TA, *Mesorhizobium* sp. strain LUK  $\beta$ -transaminase; PLP, pyridoxal 5'-phosphate; PMP, pyridoxamine-5'-phosphate; TA, transaminase; Vf- $\omega$ TA, *Vibrio fluvialis*  $\omega$ -transaminase.

\* Corresponding author at: College of Pharmacy, Chung-Ang University, Dongjak-gu, Seoul 06974, Republic of Korea.

E-mail address: [xrayleox@cau.ac.kr](mailto:xrayleox@cau.ac.kr) (H.H. Park).

## 1. Introduction

Over the last three decades, transaminases (TAs, also called amino-transferases) have been some of the most popular enzymes among structural biologists and protein engineers, owing to their unique

enzymatic properties and industrial applicability [1–4]. TAs catalyze the reversible transfer reaction of an amino group between two compounds [1]. For catalysis, amino acids and amines devoid of a carboxylic acid group constitute amino group donors, whereas ketones, keto acids, and aldehydes act as amino group acceptors. This “ping-pong” reaction is mediated by the cofactor, pyridoxal 5'-phosphate (PLP), which is located at the active site. Thus, TAs recognize two disparate compounds as their substrates at the same active site.

TAs can be classified according to the amino group position of their donor substrates ( $\alpha$ ,  $\beta$ ,  $\gamma$ , or  $\omega$ ) [5,6]. TAs recognizing an amino group bound to  $\alpha$ ,  $\beta$ , or  $\gamma$  carbon atoms are called  $\alpha$ ,  $\beta$ , and  $\gamma$ TAs, respectively.  $\omega$ TA is the common name of the TAs that recognize an amino group bound to non- $\alpha$  carbon in the donor substrate [5,6]. TAs also have the ability to distinguish between *R*- and *S*-enantiomers, signifying that the substrates are precisely recognized at the active site [7–10]. On account of such enzymatic diversity and specificity, TAs have been utilized as biocatalysts to produce useful compounds in fine chemical and pharmaceutical industries [3,11,12]. TAs, especially  $\omega$ TAs, have been applied industrially for both kinetic resolution and asymmetric synthesis of key compounds [11]. To attain kinetic resolution, undesired amine enantiomers occupying half of racemic compounds are converted to ketone products, leaving only desired enantiomers in the initial racemic form [11]. However, for asymmetric synthesis, an amino group is transferred mainly to ketone compounds selected as precursors, yielding target chiral amines [11].

PLP is a vital molecule directly involved in both the acceptance and donation of an amino group. The transamination reaction occurs through two sequential half reactions via PLP: 1) the oxidative deamination of an amino group donor and 2) the reductive amination of an amino group acceptor [4,13,14]. PLP is associated with both reactions, as a mediator of the amino group. The transamination reaction is triggered by exchanging the amino group from the donor substrate with the  $\epsilon$ -amino group of an adjacent Lys residue covalently bound to the C4' atom on PLP, thus converting PLP to pyridoxamine-5'-phosphate (PMP). Subsequently, the amino group of PMP is transferred to the acceptor substrate, yielding a new amine or amino acid. In addition to its role as a catalysis mediator, PLP also constitutes a spatial criterion for the compartmentalization of the active site pocket. Previous structural studies have shown that the active site of TAs is composed of two pockets, the P- and O-pockets [3,6,15]. As indicated by their names, the P-pocket is positioned near the phosphate group of PLP, and the O-pocket is formed in the vicinity of the O3' atom of PLP. The respective pockets exhibit diversity in terms of size and hydrophobicity depending on the type of TAs [3,14]. Hence, PLP constitutes a key molecule, with a profound impact on the structure and function of TAs.

To date, a number of TA, mainly fold type I TA structures have been determined by X-ray crystallography. Numerous structures of  $\alpha$ TAs such as aspartate aminotransferases have been reported and their mechanisms have been discussed [16–22]. Such  $\alpha$ TAs mainly recognize  $\alpha$ -amino acids and  $\alpha$ -keto acids as their substrates. However,  $\omega$ TAs recognize a wider range of substrates, compared with  $\alpha$ TAs [16–22].  $\beta$ TAs also have enzymatic activity toward  $\beta$ -amino acids, which are rare compounds in nature. In this review, thus, we deal with non- $\alpha$ TAs, namely  $\omega$ TAs including a  $\beta$ TA. Although most of TA structures are holo forms containing PLP, a small number of apo forms have also been described. In  $\omega$ TAs from *Chromobacterium violaceum* (Cv- $\omega$ TA) [23] and *Vibrio fluvialis* (Vf- $\omega$ TA) [24,25], both the apo and holo forms have been reported and their structural differences characterized. Apo [26] and holo [27] forms of a  $\beta$ TA from *Mesorhizobium* sp. strain LUK (Ms- $\beta$ TA) have also been reported. As such, comparative studies encompassing a wide range of TA structures, provide valuable information on structural differences between TA types, which allows us to infer structural dynamics.

Herein, we review previous studies on the conformational changes of fold type I TAs, with a particular focus on the effect of PLP and the substrate on the structural stability of TAs. In addition, we will address a

recent issue regarding how surface electrostatic potential contributes to substrate induction into the active site of TAs, by assessing electrostatic properties. Thus, this review provides novel insights into not only the structural dynamics of TAs to adopt adequate conformations in accordance with environmental changes, but also the transfer routes of PLP and TA substrates.

## 2. Architecture of TAs

### 2.1. Typical Overall Structure

In general, TAs belong to the two fold types (I and IV) of PLP-dependent enzymes [6]. With the exception of three TA groups, such as D-amino acid TAs, branched-chain TAs, and (*R*)-amine TAs, all TAs belong to fold type I [6]. Each TA has a specific amino donor and amino acceptor as its substrate. Such enzymatic specificity has been considered the consequence of evolutionary divergence, starting from two ancestral proteins. In addition, a number of TAs exist as dimers in solution, with a monomeric molecular weight of approximately 45,000, which implies that most TAs function as a dimer in the cellular environment. However, there are some TAs that exist as tetramers or hexamers. Apparently, the multimeric state of TAs depends on the species from which they originate. We summarize the profiles of TAs mentioned in this review in Table 1. As a typical TA structure, here we briefly describe the overall structure of an  $\omega$ TA from *C. violaceum* (Cv- $\omega$ TA; PDB ID: 4A6T), which is categorized as a fold type I TA and functions as a dimer [23].

Cv- $\omega$ TA is a good model in terms of its structural diversity, since its four crystal structures have been determined, of which two are the apo form, one is the holo form, and the remaining structure is a mixture of the apo and holo forms. Cv- $\omega$ TA exists as a dimer both in solution and in the crystal environment (Fig. 1A). Each subunit of the dimer consists of two domains: a large domain and a small domain (Fig. 1B). The large domain adopts a three-layered  $\alpha/\beta/\alpha$  sandwich fold, with a central parallel  $\beta$  sheet. The small domain is subdivided into an N-terminal lobe and a C-terminal lobe, which are linked to the large domain. It is noteworthy that the two lobes of the small domain spatially combine with each other, even though their amino acid sequences are discontinuous.

### 2.2. Active Site Chemistry

The active site of TAs is located at the interface between two subunits and simultaneously, between two domains, with a PLP molecule positioned at the bottom (Fig. 1C). In the “resting period” of the catalytic cycle, PLP forms a Schiff base by covalently binding to an adjacent Lys residue. It is a striking structural feature of TAs that some residues from one subunit are directly involved in the formation of the active site of the other subunit. This is the rationale for the need of TAs to form oligomers to properly function as enzymes [16,28]. The PLP-binding site is located somewhat far from the entrance of the active site, resulting in a relatively deep funnel toward the active site (Fig. 1D). Surface electrostatic potential analysis has revealed that positively charged residues are predominantly distributed on the active site funnel (as discussed in more detail in Section 5). These structural traits described above are well conserved among TAs (Fig. 1E).

In the crystal structure of the holo form of Cv- $\omega$ TA, PLP links to the Lys288 residue, indicating that the structure is a snapshot of the resting period. UV-visible spectrometric analysis can be used to determine whether the cofactor is PLP or PMP, because the respective molecules show different absorption spectra. Previous studies have demonstrated that the PLP-bound form exhibits an absorption peak at approximately 420 nm, whereas the PMP-bound form has an absorption peak at approximately 330 nm [29,30]. UV-visible absorption spectra, thus, provide information on a corresponding step in the whole catalytic cycle. The PLP cofactor interacts with neighboring residues and water molecules (Fig. 1F). The three oxygen atoms in the phosphate group of PLP form salt bridges with Gly120, Ser121, and Thr321. The carbon atoms

**Table 1**  
Transaminase profiles.

Transaminase	Organism	Multimeric state	Cofactor	Bound molecule	PDB ID	Reference
Cv- $\omega$ TA	<i>Chromobacterium violaceum</i>	Dimer	Apo	Polyacrylic acid	4A6R	23
		Dimer	PLP		4A6T	23
		Dimer	Apo		4AGU	23
		Dimer	Apo/PLP		4A72	23
Vf- $\omega$ TA	<i>Vibrio fluvialis</i> JS17	Dimer	PMP		4E3Q	24
		Dimer	PLP		4E3R	24
		Dimer	Apo		5ZTX	25
		Dimer	PLP		2YKU	27
Ms- $\beta$ TA	<i>Mesorhizobium</i> sp. strain LUK	Dimer	PLP	2-aminooxyacetic acid	2YKV	27
		Dimer	PLP	2-oxoglutaric acid	2YKX	27
		Dimer	PLP	(S)- $\beta$ -phenylalanine	2YKY	27
		Dimer	PLP	(R)-3-amino-5-methylhexanoic acid	4AO4	27
		Dimer	Apo		6IZ9	26
Mt-TA	<i>Mycobacterium tuberculosis</i>	Dimer	PLP		2CIN	33
		Dimer	PLP	Lysine	2CJD	33
		Dimer	PMP		2CJG	33
		Dimer	PLP	2-oxoglutaric acid	2CJH	33
Hp-TA	<i>Helicobacter pylori</i>	Dimer	Apo		2FN6	34
		Dimer	PLP		2FNI	34
As-TA	<i>Arthrobacter</i> sp. KNK168	Dimer	PMP	Uridine-diphosphate-N- acetylglucosamine	2FWH	35
		Dimer	PLP		3WWI	35
		Dimer	PLP		3WWJ	35
Tu-TA	<i>Thermoproteus uzonensis</i>	Dimer	PLP		5CE8	30
Go-TA	<i>Gluconobacter oxydans</i>	Dimer	PLP			36, 37
Li-TA	<i>Lactococcus lactis</i>	Dimer	PLP			38
Pa-TA	<i>Pseudomonas aeruginosa</i>	Tetramer	PLP			39
Vm-TA	<i>Vulcanisaeta moutnovskia</i>	Tetramer	PLP			40
Pp-TA	<i>Pseudomonas putida</i>	Tetramer	PLP		3A8U	41
MI-TA	<i>Mesorhizobium loti</i>	Tetramer			229U	42
		Tetramer		Pyridoxamine	229V	42
		Tetramer		Pyridoxal	229W	42
Ma-TA	<i>Methanococcus aeolicus</i>	Hexamer	PLP			43
Ss-AT	<i>Sus scrofa</i>	Dimer	PLP		5VK7	31
hOAT	<i>Homo sapiens</i>	Dimer	PLP			53
AroAT	<i>Paracoccus denitrificans</i>	Dimer	PLP			
		Dimer	PLP	Maleic acid	1AY4	17
		Dimer	PLP	3-phenylpropionic acid	1AY5	18
		Dimer	PLP	Histidinol-phosphate	1AY8	18
HspAT	<i>Escherichia coli</i>	Dimer	PLP	N-(5'-phosphopyridoxyl)-L- glutamate	1GEW	19
		Dimer	PLP		1GEX	19
GlnAT	<i>Thermus thermophilus</i> HB8	Dimer	PLP		1GEY	19
		Dimer	PLP		1V2D	20
AcOAT	<i>Thermus thermophilus</i> HB8	Dimer	PLP		1V2F	20
		Dimer	PLP	N-(5'-phosphopyridoxyl)-N $\alpha$ - acetyl-L-ornithine	1VEF	16
		Dimer	PLP	N-(5'-phosphopyridoxyl)-L- glutamate	1WKG	16
BCAT	<i>Escherichia coli</i>	Dimer	PLP		1WKH	16
		Dimer	PLP	4-methylvalerate	1I1K	21
		Dimer	PLP	Glutamate	1I1M	21
		Dimer	PLP		1IYE	22

on PLP also form hydrophobic interactions with adjacent hydrophobic residues, such as Tyr153, Gly155, Val261, Ile262, and Phe320. The C4' atom on the PLP ring covalently binds to the  $\epsilon$ -amino group of the Lys288 residue. In addition, four water molecules are also involved in PLP coordination. The phosphate group interacts with three water molecules, two of which mediate the interaction between the oxygen atoms of the phosphate group and the backbone atoms of Asn118, Gly319, and Tyr322. The oxygen atom on the aromatic ring also forms a network with Glu226 and Ala231 mediated by a water molecule. Overall, the PLP cofactor is fixed by forming many hydrogen bonds and hydrophobic interactions with neighboring residues and water molecules. Notably, Gly319, Thr321, and Tyr322 from the other subunit also contribute to PLP fixation. Such active site chemistry signifies that the dimer of TAs is the minimum functional unit required for catalytic activity.

In addition, given that transamination is achieved by chemical reactions such as nucleophilic substitution and general base catalysis, the protonation states of PLP and adjacent residues, along with the geometry in the active site, are crucial for catalysis. Recent studies have shown the protonation states in the active site and the geometry of the Schiff base linked to the pyridine ring [31,32]. Dajnowicz et al.

determined the neutron crystal structure of an aspartate aminotransferase from *Sus scrofa*, in which one subunit and the other subunit showed the internal aldimine form and external aldimine form, respectively [31]. In the internal aldimine form, the C4' atom of PLP covalently binds to the  $\epsilon$ -amino group of Lys258, whereas the C4' atom of PLP is covalently linked to the C $\alpha$  atom of  $\alpha$ -methylaspartate in the external aldimine form. The authors showed that the deprotonated nitrogen atom of the Schiff base in the internal aldimine form adopts non-planarity to the pyridine ring, and hyperconjugation between the  $\sigma$  orbital and empty or partially occupied antibonding  $\pi$  orbital of the Schiff base contributes to stabilization of the ground state of the external aldimine [31,32].

Another noticeable structural feature of the active site is that it consists of two pockets (P- and O-pockets), which are different in size, depending on the fold type and class of TAs [5,13,15,27]. As shown in Fig. 1C, these pockets are also observed in Cv- $\omega$ TA. These spatial differences restrict the size and orientation of the functional groups of the substrate upon the enzyme-substrate complex formation. In other words, the bulkier functional groups of the substrate are oriented towardst the large pocket, whereas the smaller functional groups are

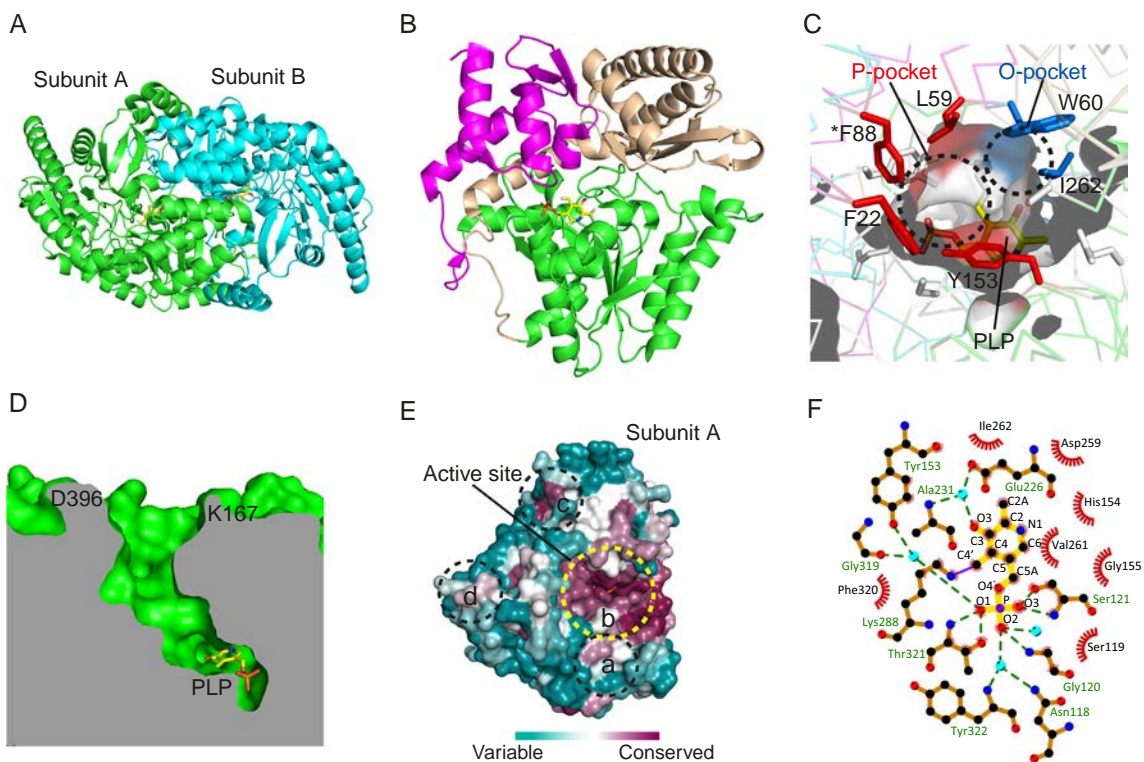


**Fig. 1.** Structure of Cv- $\omega$ TA. (A) Overall structure. PLP molecules are represented as yellow sticks. (B) The two domains of subunit A: large domain (green) and small domain. The small domain is divided into N- (magenta) and C-terminal lobes (wheat) (C) Zoomed-in view of the active site comprising the P- and O-pockets. The colour code is the same as that of panel (B). Subunit B is colored blue. The asterisk of F88 denotes that it originates from the other subunit. The white sticks represent residues involved in PLP fixation. (D) A cross-sectional view showing a funnel to the active site. (E) Surface representation of subunit A colored by the degree of sequence conservation. Regions a-d correspond to high conservation regions. (F) Diagram of PLP interactions in the active site. The blue circles represent water molecules.

assigned to the small pocket, thus satisfying a structural orientation of prerequisites required for enantioselectivity [5,13,15,27].

### 2.3. Multimeric State as a Functional Unit

It is well known that TAs play biological roles as multimeric forms. They can form dimers, tetramers, and hexamers, depending on the species from which they originate. A number of biochemical studies have demonstrated multimeric states of TAs in solution, implying that they are functional units in the cellular environment. A dimeric form in solution is observed for TAs from *Mycobacterium tuberculosis* (PDB ID: 2CIN, 2CJD, 2CJG, and 2CJH) [33], *Helicobacter pylori* (PDB ID: 2FN6, 2FNI, and 2FNU) [34], *Mesorhizobium* sp. strain LUK (PDB ID: 2YKU, 2YKV, 2YKX, 2YKY, 4AO4, and 6IZ9) [26,27], *Arthrobacter* sp. KNK168 (PDB ID: 3WWH, 3WWI, and 3WWJ) [35], *Chromobacterium violaceum* (PDB ID: 4A6R, 4A6T, 4A6U, and 4A72) [23], *Vibrio fluvialis* JS17 (PDB ID: 4E3Q, 4E3R, and 5ZTX) [24,25], *Thermoproteus uzonensis* (PDB ID: 5CE8) [30], *Gluconobacter oxydans* [36,37], and *Lactococcus lactis* [38]. However, TAs from *Pseudomonas aeruginosa* [39], *Vulcanisaeta moutnovskia* [40], *Pseudomonas putida* (PDB ID: 3A8U) [41], and *Mesorhizobium loti* (PDB ID: 2Z9U, 2Z9V, and 2Z9W) [42] exist as tetramers in solution and in a crystal environment. Lastly, a TA from *Methanococcus aeolicus* forms a hexamer in solution [43].

It is not fully understood why TAs exist as diverse multimeric forms such as dimers, tetramers, and hexamers in solution, depending on their fold type or host species. Alternatively, it is worth investigating whether TAs maintain their unique multimeric states, taking into account the fact that the active site is formed at the interface between subunits. Hence, TAs should retain at least a dimeric state to properly function as an enzyme. A recent study showed that the dissociation of PMP from a PMP-bound TA results in aggregation of the TA, by forming unstable

apoenzymes and the dissociation rate of PMP is faster in the dimeric form than in the tetrameric form [44]. The authors also found that the cofactor can bind more tightly to the neighboring residues when the TA is in the tetrameric state than when it is in the dimeric state. However, it is not clear whether dimeric TAs are exposed to a cellular environment that restricts the dissociation of PMP. If tetrameric TAs do not have other options to avoid enzymatic inactivation by the dissociation of PMP, their unique tetramer formation may be a consequence of evolutionary adaptation to maintain a stable state.

### 3. Structural Differences Between the Apo and Holo Forms

Previous studies have reported the effect of PLP on the structure and function of TAs by comparing structures between apo and holo forms [23,25,26]. Humble et al. determined the apo (PDB ID: 4A6R; apo1 and 4A6U; apo2) and holo (PDB ID: 4A6T) structures of Cv- $\omega$ TA [23]. This crystallographic study provides valuable information on structural differences, in that the crystal structures revealed conformational diversity in response to molecules incorporated in the active site. In the apo2 structure, three regions (R5–A33 and G152–P178 from chain A and I311–F320 from chain B) are disordered, but are ordered in the holo form (Fig. 2A; black dashed oval). These disordered regions corresponding to 66 residues, indicate that they are highly flexible in the apo form. These regions are important because they constitute the components of the active site. Furthermore, some of the active site-forming residues from the other chain (T321–S323 from chain B) show different spatial positions between the apo and holo forms (Fig. 2A; red dashed oval). These results suggest that PLP incorporation results in structural rearrangement and stabilization of the disordered regions, thereby forming the complete active site.

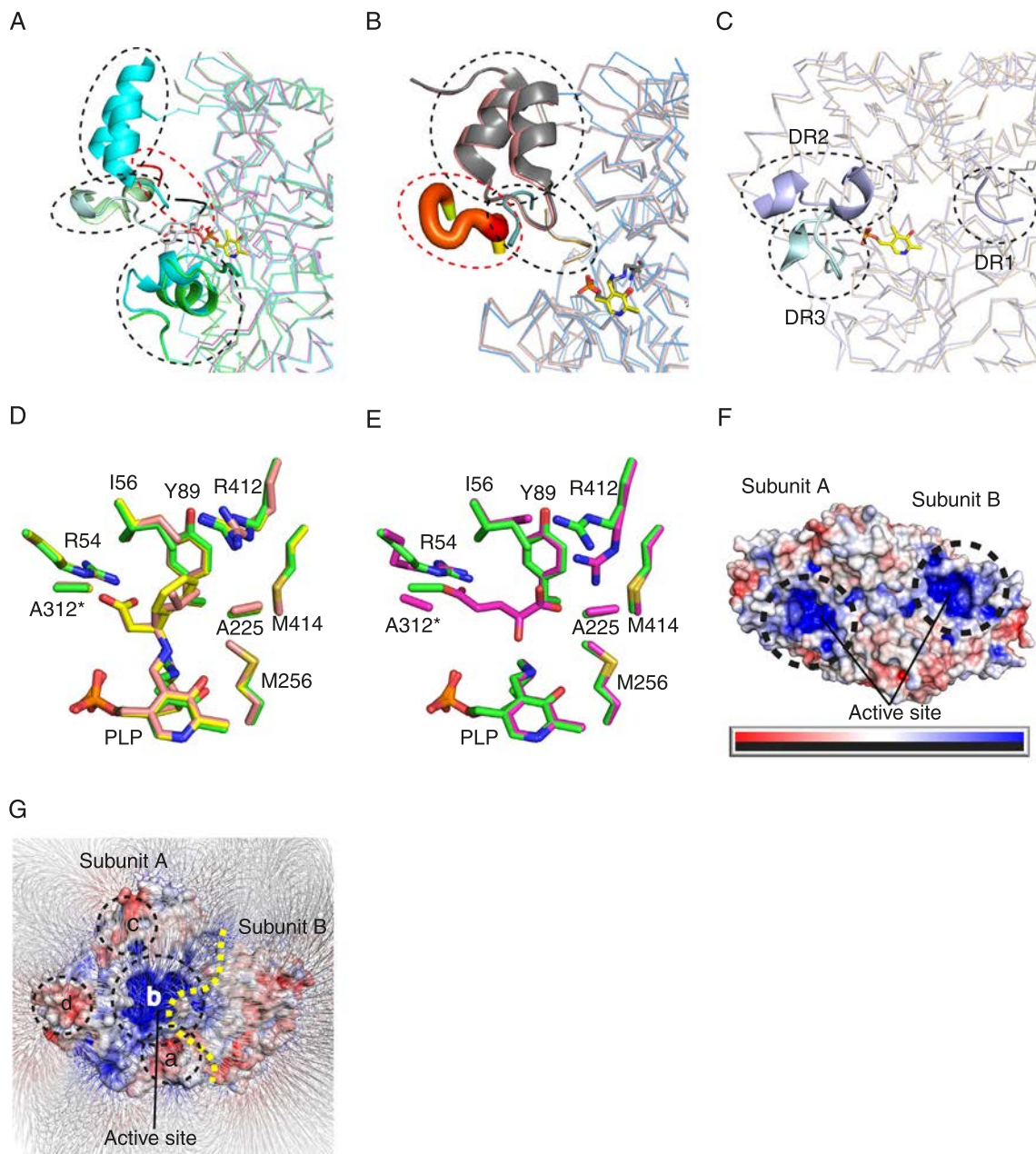


**Fig. 2.** Structural comparison and surface electrostatic properties. Structural comparison between the apo and holo forms of (A) Cv- $\omega$ TA, (B) Vf- $\omega$ TA, and (C) Ms- $\beta$ TA, with a focus of the active site. Apo1 (chain A: green; chain B: light green), apo2 (chain A: magenta; chain B: red), and holo (chain A: cyan; chain B: light cyan and black) forms of Cv- $\omega$ TA; apo (chain A: marine; chain B: light teal and rainbow putty showing B-factor values), PLP-bound (chain A: grey; chain B: light grey), and PMP-bound (chain A: salmon; chain B: bright orange) forms of Vf- $\omega$ TA; apo (chain A: wheat) and holo (chain A: light blue; chain B: pale cyan) forms of Ms- $\beta$ TA. Active site residues of the native form (D: green) of Ms- $\beta$ TA and the forms complexed with (S)- $\beta$ -phenylalanine (D: yellow), (R)-3-amino-5-methylhexanoic acid (D: tint), and 2-oxoglutarate (E: magenta). The asterisk of A312 denotes that it originates from the other subunit. (F) Surface electrostatic potential of Ms- $\beta$ TA. The scale bar indicates a range from -5kT/e (red) to 5kT/e (blue). (G) Electric field generated by Ms- $\beta$ TA. The electric field map grade is contoured at the -0.5 σ level. Regions a-d correspond to those in Fig. 1E. The yellow dashed line denotes a boundary line between subunit A and B.

It is also noteworthy that the structures of apo1, containing a tetramer of poly(acrylic acid) near the active site and apo2 are different from each other. In the apo1 structure, some residues (residues G152–H170 and D174–P178 form chain A and I311–F320 from chain B) are ordered (Fig. 2A; black dashed oval). This may be the consequence of structural stabilization induced by poly(acrylic acid). In apo1, however, the neighboring-chain region observed in the holo form (I311–F320 from chain B) adopts similar spatial coordinates to those in apo2, rather than those in the holo form. This means that only PLP can induce the conformational change of the corresponding region to complete the specific active site architecture.

A comparative study of the apo and holo forms of Vf- $\omega$ TA also showed a similar structural pattern to Cv- $\omega$ TA [25]. The holo forms of Vf- $\omega$ TA were reported as two types: PLP-bound and PMP-bound types [24]. However, although the chemical state of the cofactor was different, significant structural differences between the two types were not found. In the apo structure, the region corresponding to Asn2–Lys28 from chain A is disordered (Fig. 2B; black dashed circle) and the spatial arrangement of the active site-forming residues from chain B (F321–G325) is different from those in the holo forms, which are located in the proximity of the cofactor (Fig. 2B; black dashed oval). In particular, the neighboring-chain residues (I311–P318 from chain B) exhibit high

B-factor values (Fig. 2B; red dashed oval), implying that this region may retain structural plasticity in the apo form to facilitate transformation into the holo form.

In addition, the effect of PLP on active site formation has been reported in a structural study comparing the apo form and the holo form of a  $\beta$ -transaminase from *Mesorhizobium* sp. strain LUK [26]. Three major disordered regions (DR1–3) found near the active site in the apo form are ordered in the holo form (Fig. 2C). While DR1 (residues 1–16) and DR2 (residues 48–59) are from chain A, DR3 (residues 300–311) is from chain B. The active site architecture in the apo form is assumed to be flexible owing to the three DR regions, whereas that in the holo form is specific for the substrate binding. Thus, PLP is assumed to contribute to the structural stabilization of the DR regions, resulting in the formation of a precise active site. As discussed in this structural study paper [26], considering that the DR regions adopt diverse conformers in the absence of PLP, each appropriate conformer may be selected upon binding to PLP, exhibiting the minimum in the free energy continuum. If this hypothesis is correct, the “disorder-to-order transition” phenomenon can be explained by the conformational selection theory [45–50].

These results above are based on structural information obtained by X-ray crystallography. Although X-ray structures provide valuable information on protein dynamics, it should be noted that structures in crystal environments could be different from those in solution. Some literatures have pointed out structural discrepancy of identical proteins between X-ray and NMR structures [51,52]. These studies indicate that interpreting protein dynamics from X-ray structures on both large and small scales is based on a premise of somewhat confined crystal environments.

Finally, a biochemical study has been reported evaluating differences in thermal stability between the apo and holo forms of PLP-dependent human ornithine  $\delta$ -aminotransferase (hOAT) [53]. The authors performed biochemical analyses, such as analytical ultracentrifugation, size exclusion chromatography, and circular dichroism to investigate the multimeric state and thermal stability of the apo and holo forms of hOAT. The apo and holo forms were shown to have  $T_m$  values of 46 °C and 67 °C, respectively, and the apo form was found to be more susceptible to denaturation and aggregation than the holo form. In addition, the tetrameric apo form was more resistant to denaturation and aggregation than the dimeric apo form. These results demonstrate that PLP plays a vital role in the structural stabilization of hOAT and the degree of interaction between subunits is associated with maintaining its intrinsic structure.

#### 4. Dual Substrate Recognition Mechanism

TAs have the enzymatic property to exploit two different kinds of substrates at the same active site. Such a fact allows us to investigate structural differences between an amino group donor-bound form and an amino group acceptor-bound form. A structural study on substrate-bound structures of Ms- $\beta$ TA provides insights into the dual substrate mechanism of TAs [27]. Wybenga et al. determined crystal structures of Ms- $\beta$ TA in complex with its substrates, including (S)- $\beta$ -phenylalanine, (R)-3-amino-5-methylhexanoic acid, 2-oxoglutarate, and its inhibitor [27]. In all the tested complexes, the respective functional groups of the substrates were found to interact with the appropriate side chains of key residues in the active site. In the complex with (S)- $\beta$ -phenylalanine, the carboxylic acid group forms a salt bridge with Arg54, whereas the phenyl group interacts with hydrophobic residues, such as Ile56, Tyr89, Ala225, Met256, Met414 (from one subunit), and Ala312 (from the other subunit, Fig. 2D, yellow). (R)-3-amino-5-methylhexanoic acid, retaining the aliphatic chain, constitutes a comparative object with the aromatic compound, (S)- $\beta$ -phenylalanine, in terms of chemical properties. In the (R)-3-amino-5-methylhexanoic acid-bound structure, the functional groups of the substrate are oriented in the same mode as those of (S)- $\beta$ -phenylalanine (Fig. 2D,

tint). The 2-oxoglutarate-bound form, however, shows a somewhat different pattern of interaction. Contrary to the two substrates discussed above, the  $\alpha$ -carboxylic acid group of 2-oxoglutarate forms a salt bridge with Arg412 (Fig. 2E, magenta). The keto oxygen atom is oriented toward the nitrogen atom of Lys280, which is covalently bound to PLP.

Structural comparison studies have identified subtle structural differences between the two amino group donor complexes and the amino group acceptor complex. While no significant structural differences were found between the (S)- $\beta$ -phenylalanine-bound form and the (R)-3-amino-5-methylhexanoic acid-bound form, the binding of 2-oxoglutarate gave rise to spatial rearrangements of Ala312 and Arg412. When complexed with 2-oxoglutarate, the position of Ala312 deviates somewhat from the  $\gamma$ -carboxylic acid group of 2-oxoglutarate, maintaining a distance of 3.5 Å. This may occur to avoid a steric clash that would happen if Ala312 did not deviate spatially. It is also noteworthy that the position of Arg412 is adjusted to form a salt bridge with the  $\alpha$ -carboxylic acid group of 2-oxoglutarate. Comparative analysis of Ms- $\beta$ TA shows that some residues in the active site are precisely rearranged in response to substrates. Thus, the dual substrate recognition of Ms- $\beta$ TA can be explained by the induced fit mechanism, by which it has been described that structural changes of enzymes occur upon binding to their substrates [54].

The induced fit mechanism has also been exploited to explain a domain movement observed in aspartate aminotransferases [55,56] from *Escherichia coli*. It is well known that many TAs undergo a large conformational change from an open to a closed form upon the binding of the substrate [16]. This conformational change occurs by the access of the small domain to the active site entrance. In the closed form, the active site is covered with part of the small domain, precluding outer water molecules from entering the active site [16].

As another dual substrate recognition mechanism, the lock and key model, along with the induced fit model, has been proposed by Hirotsu et al. to describe the dual substrate recognition mechanism of TAs [16]. The lock and key model, first suggested by Emil Fischer in 1894 is the theory that enzymes bind complementarily to their substrates for catalysis as a key (substrate) fits precisely into a lock (enzyme). Based on X-ray crystallographic studies, they analyzed the following TA structures: 1) aromatic amino acid aminotransferase from *Paracoccus denitrificans* (AroAT) (PDB ID: 1AY4) [17] and its maleate (PDB ID: 1AY5) and 3-phenylpropionate (PDB ID: 1AY8)-bound forms [18], 2) histidinol-phosphate aminotransferase from *E. coli* (HspAT; PDB ID: 1GEW) and its histidinol-phosphate- (PDB ID: 1GEX) and N-(5'-phosphopyridoxyl)-L-glutamate (PDB ID: 1GEY)-bound forms [19], 3) glutamine-phenylpyruvate aminotransferase from *Thermus thermophilus* HB8 (GlnAT; PDB ID: 1V2D) and its 3-phenylpropionate (PDB ID: 1V2F)-bound form [20], 4) acetylornithine aminotransferase from *Thermus thermophilus* HB8 (AcoAT; PDB ID: 1VEF) and its N-(5'-phosphopyridoxyl)-N $\alpha$ -acetyl-L-ornithine- (PDB ID: 1WKG) and N-(5'-phosphopyridoxyl)-L-glutamate (PDB ID: 1WKH)-bound forms [16], and 5) branched-chain amino acid aminotransferase from *E. coli* (BCAT; PDB ID: 1I1K) and its 4-methylvalerate (PDB ID: 1I1M) [21] and glutamate (PDB ID: 1IYE)-bound forms [22]. The authors observed that salt bridge formation between residues and substrates in the active site, along with a hydrogen bond network as required, are involved in the rearrangements of the key residues. They concluded that AroAT recognizes dual substrates via the induced fit mechanism, whereas BCAT utilizes the lock and key mechanism to recognize its substrates. In the cases of HspAT, GlnAT, and AcoAT, dual substrate recognition occurs by a combination of the two mechanisms, although they differ in their dependence on each mechanism.

#### 5. Electrostatic Steering for Cofactor and Substrate Binding

Surface electrostatic analysis of Ms- $\beta$ TA has revealed that positively charged residues are dominantly distributed at the active site, whereas

negatively charged residues are sparsely distributed in adjacent regions of the entrance to the active site (Fig. 2F) [26]. It is possible that this distribution pattern is generalized for all TAs, considering that the corresponding residues are evolutionarily conserved (Fig. 1E). Such a unique surface feature signifies that it can generate a potent electric field, thereby attracting negatively charged molecules into the active site. As an example, electric field formation around Ms- $\beta$ TA has been described using the Adaptive Poisson-Boltzmann Solver [57] (Fig. 2G). It is also noteworthy that PLP and amino group acceptors, such as pyruvate or 2-oxoglutarate, retain strong negative charges. Accordingly, it is reasonable to assume that PLP and substrates as amino group acceptors are attracted into the active site by the electric field. This phenomenon has been called electrostatic steering [58–60]. For amino group donors such as amino acids, considering that they are zwitterions, mostly retaining a net charge of 0, simple diffusion rather than electrostatic steering is assumed to constitute a driving force for access to the active site.

Due to the nature of the electrical phenomenon around proteins, however, it is difficult to experimentally verify the electrostatic steering mechanism with biophysical measurements. However, previous studies using computational analyses, such as Brownian dynamics (BD); electrostatic calculations based on the Poisson-Boltzmann equation; electrostatic potential similarity analysis, along with site-directed mutagenesis, have shown that this mechanism is plausible [58–63]. Based on the results of these studies, it has been concluded that electrostatic properties in the vicinity of the substrate-binding sites of enzymes, such as superoxide dismutase, acetylcholinesterase, and barnase, give rise to electrostatic steering for substrate binding. These studies have also shown that the introduction of charged residues to the active site increases the rate of association of these enzymes with their respective substrates, implying that the results may be due to enhanced electrostatic potential [59,61,62]. These results also agree with predictions from BD simulations, based on the finite-difference linearized Poisson-Boltzmann equation. Therefore, surface electrostatic potential analysis of TAs constitutes circumstantial evidence to support the electrostatic steering phenomenon.

Although we here present the electrostatic steering model as a possible scenario, other possibilities need to be explored. For example, it might be possible that PLP insertion into the active site is mediated by a PLP-delivery protein, or insertion of amino group acceptors along with PLP is achieved by simple diffusion. In addition, the electrostatic steering mechanism may not be applied to all PLP-dependent enzymes. At the present stage of our knowledge, the actual PLP and substrate insertion mechanism still remains elusive.

## 6. A Possible Working Mechanism of TAs

On the basis of these biochemical and structural studies of TAs, we here propose the following working mechanism of TAs, including PLP and substrate insertion into the active site (Fig. 3).

- (i) A multimeric functional unit, such as a dimer, is formed via the assembly of monomers.
- (ii) An electric field generated around the TA induces the insertion of PLP into the active site. Flexible active site architecture facilitates PLP incorporation. Conformational selection and induced fit models are associated with this step.
- (iii) An amino group donor substrate binds to the active site pocket. Diffusional collision drives the amino group donor into the active site. The lock and key and induced fit mechanisms are applied at this step.
- (iv) The primary by-product, upon the formation of PMP, is expelled from the active site.
- (v) An amino group acceptor substrate binds to the active site pocket. The electric field plays the same role as in step (ii). The lock and key and induced fit mechanisms are involved in this step.

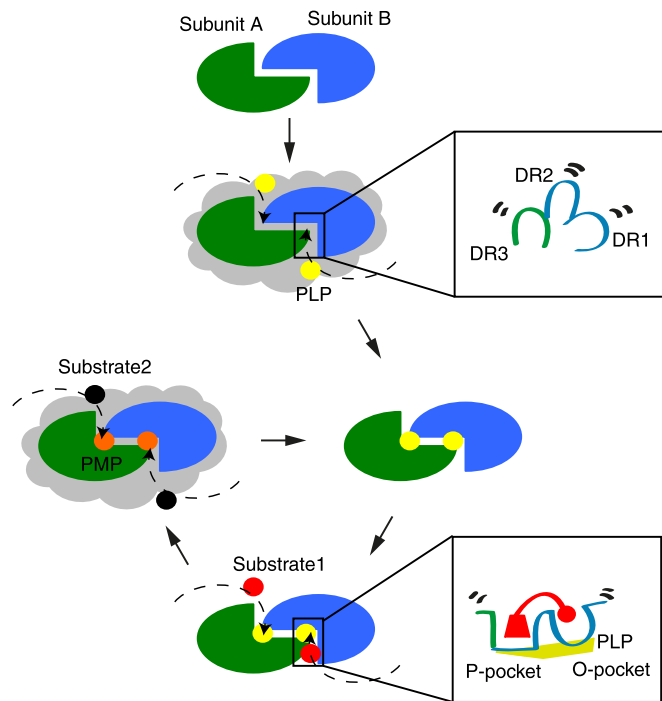


**Fig. 3.** A possible working mechanism of TAs. The grey regions denote electric fields generated by the TA. The curved arrows indicate routes for transport of PLP and substrates to the active site.

- (vi) The transferring of the amino group from PMP gives rise to the final product.
- (vii) The final product is expelled from the active site.

## 7. Summary and Outlook

The crystal structures of fold type I TAs, determined by X-ray crystallography, have provided significant information on the details of the active site, as well as the overall architecture of the enzymes. Based on comparative analyses of the structures of native forms and substrate-bound forms, it has been found that residues forming the active site are precisely rearranged and simultaneously undergo local conformational changes upon PLP and substrate binding. The specific and diverse substrate selectivity of fold type I TAs, along with PLP insertion, is an evolutionary consequence of adopting their unique structures. However, despite the valuable information accumulated thus far on the structure and function of fold type I TAs, investigations of TA structural dynamics have depended on structural comparison and B-factor analysis. These analyses allow us to infer conformational changes corresponding to the respective steps in the catalytic cycle and provide information on their intrinsic mobility. Nevertheless, some outstanding issues remain to be resolved. For example, it is not clear which pathway is involved in the structural stabilization of the active site by PLP during the “disorder-to-order transition” phenomenon. Moreover, it still remains elusive whether tetrameric or hexameric TAs take catalytic advantages over dimeric TAs by maintaining structural stability. In addition, the TA structures that have been characterized to date include those from psychrophilic, thermophilic and hyperthermophilic organisms as well as mesophilic organisms. This diversity, in terms of thermostability, gives us an opportunity to investigate structural determinants affecting thermal tolerance. Although structural determination of TAs has depended on X-ray crystallography thus far, it is possible that their real movements in the cellular environment could be different from results observed by X-ray crystallography. Integrated analytical methods including computational methods, such as molecular

dynamics simulation, along with biochemical and biophysical analyses, may solve the remaining enigmas concerning TAs.

## Funding Source

This work was supported by National Research Foundation of Korea (NRF) grant funded by the Korea government (NRF-2017M3A9D8062960 and NRF-2018R1A4A1023822).

## Declaration of Competing Interest

The authors declare no competing interests.

## Acknowledgements

The authors thank Mr. Chang Min Kim and Miss Hyun Ji Ha for helping the collection of references.

## References

- [1] Cooper AJ, Meister A. An appreciation of professor Alexander E. Braunstein. The discovery and scope of enzymatic transamination. *Biochimie* 1989;71(4):387–404.
- [2] Hayashi H. Pyridoxal enzymes: mechanistic diversity and uniformity. *J Biochem* 1995;118(3):463–73.
- [3] Slabu I, Galman JL, Lloyd RC, Turner NJ. Discovery, engineering, and synthetic application of transaminase biocatalysts. *ACS Catal* 2017;7(12):8263–84.
- [4] Toney MD. Controlling reaction specificity in pyridoxal phosphate enzymes. *Biochim Biophys Acta* 2017;1814(11):1407–18.
- [5] Malik MS, Park ES, Shin JS. Features and technical applications of  $\omega$ -transaminases. *Appl Microbiol Biotechnol* 2012;94(5):1163–71.
- [6] Bezsdudnova EY, Boyko KM, Popov VO. Properties of bacterial and archaeal branched-chain amino acid aminotransferases. *Biochemistry (Mosc)* 2017;82(13):1572–91.
- [7] Soda K, Yoshimura T, Esaki N. Stereospecificity for the hydrogen transfer of pyridoxal enzyme reactions. *Chem Rec* 2001;1(5):373–84.
- [8] Iwasaki A, Yamada Y, Ikenaka Y, Hasegawa J. Microbial synthesis of (R)- and (S)-3,4-dimethoxyphetamines through stereoselective transamination. *Biotechnol Lett* 2003;25(21):1843–6.
- [9] Iwasaki A, Yamada Y, Kizaki N, Ikenaka Y, Hasegawa J. Microbial synthesis of chiral amines by (R)-specific transamination with *Arthrobacter* sp KNK168. *Appl Microbiol Biotechnol* 2006;69(5):499–505.
- [10] Koszelewski D, Tauber K, Faber K, Kroutil W.  $\omega$ -Transaminases for the synthesis of non-racemic  $\alpha$ -chiral primary amines. *Trends Biotechnol* 2010;28(6):324–32.
- [11] Fuchs M, Farnberger JE, Kroutil W. The industrial age of biocatalytic transamination. *Eur J Org Chem* 2015(32):6965–82.
- [12] Guo F, Berglund P. Transaminase biocatalysis: optimization and application. *Green Chem* 2017;19:333–60.
- [13] Park ES, Kim M, Shin JS. Molecular determinants for substrate selectivity of  $\omega$ -transaminases. *Appl Microbiol Biotechnol* 2012;93(6):2425–35.
- [14] Schiroli D, Peracchia C. A subfamily of PLP-dependent enzymes specialized in handling terminal amines. *Biochim Biophys Acta* 2015;1854(9):1200–11.
- [15] Oosterwijk NV, Willies S, Hekelaar J, Terwisscha van Scheltinga AC, Turner NJ, Dijkstra BW. Structural basis of the substrate range and enantioselectivity of two (S)-selective  $\omega$ -transaminases. *Biochemistry* 2016;55(31):4422–31.
- [16] Hirotsu K, Goto M, Okamoto A, Miyahara I. Dual substrate recognition of aminotransferases. *Chem Rec* 2005;5(3):160–72.
- [17] Okamoto A, Nakai Y, Hayashi H, Hirotsu K, Kagamiyama H. Crystal structures of *Paracoccus denitrificans* aromatic amino acid aminotransferase: a substrate recognition site constructed by rearrangement of hydrogen bond network. *J Mol Biol* 1998;280(3):443–61.
- [18] Okamoto A, Ishii S, Hirotsu K, Kagamiyama H. The active site of *Paracoccus denitrificans* aromatic amino acid aminotransferase has contrary properties: flexibility and rigidity. *Biochemistry* 1999;38(4):1176–84.
- [19] Haruyama K, Nakai T, Miyahara I, Hirotsu K, Mizuguchi H, Hayashi H, et al. Structures of *Escherichia coli* histidinol-phosphate aminotransferase and its complexes with histidinol-phosphate and N-(5'-phosphopyridoxyl)-L-glutamate: double substrate recognition of the enzyme. *Biochemistry* 2001;40(15):4633–44.
- [20] Goto M, Omi R, Miyahara I, Hosono A, Mizuguchi H, Hayashi H, et al. Crystal structures of glutamine:phenylpyruvate aminotransferase from *Thermus thermophilus* HB8: induced fit and substrate recognition. *J Biol Chem* 2004;279(16):16518–25.
- [21] Okada K, Hirotsu K, Hayashi H, Kagamiyama H. Structures of *Escherichia coli* branched-chain amino acid aminotransferase and its complexes with 4-methylvalerate and 2-methylleucine: induced fit and substrate recognition of the enzyme. *Biochemistry* 2001;40(25):7453–63.
- [22] Goto M, Miyahara I, Hayashi H, Kagamiyama H, Hirotsu K. Crystal structures of branched-chain amino acid aminotransferase complexed with glutamate and glutarate: true reaction intermediate and double substrate recognition of the enzyme. *Biochemistry* 2003;42(13):3725–33.
- [23] Humble MS, Cassimjee KE, Häkansson M, Kimburg YR, Walse B, Abedi V, et al. Crystal structures of the *Chromobacterium violaceum*  $\omega$ -transaminase reveal major structural rearrangement upon binding of coenzyme PLP. *FEBS J* 2012;279(5):779–92.
- [24] Midelfort KS, Kumar R, Han S, Karmilowicz MJ, McConnell K, Gehlhaar DK, et al. Redesigning and characterizing the substrate specificity and activity of *Vibrio fluvialis* aminotransferase for the synthesis of imagabalin. *Protein Eng Des Sel* 2013;26(1):25–33.
- [25] Shin YC, Yun H, Park HH. Structural dynamics of the transaminase active site revealed by the crystal structure of a co-factor free omega-transaminase from *Vibrio fluvialis* JS17. *Sci Rep* 2018;8(1):11454.
- [26] Kwon S, Park HH. Crystal structure of the apo form of a  $\beta$ -transaminase from *Mesorhizobium* sp. strain LUK. *Protein Sci* 2019;28(5):964–70.
- [27] Wybenga GG, Crismerau CG, Janssen DB, Dijkstra BW. Structural determinants of the  $\beta$ -selectivity of a bacterial aminotransferase. *J Biol Chem* 2012;287(34):28495–284502.
- [28] McPhalen CA, Vincent MC, Picot D, Jansonius JN. Domain closure in mitochondrial aspartate aminotransferase. *J Mol Biol* 1992;227:197–213.
- [29] Gough K, Allison G, Rogers L, Smith A. In vitro characterization of the inhibitor resistance of glutamate-1-semialdehyde aminotransferase from the cyanobacterium *Synechococcus PCCG301* GR6. *Eur J Phycol* 2002;37(3):419–28.
- [30] Boyko KM, Stekhanova TN, Nikolaeva AY, Mardanov AV, Rakitin AL, Ravin NV, et al. First structure of archaeal branched-chain amino acid aminotransferase from *Thermoproteus uzonensis* specific for L-amino acids and R-amines. *Extremophiles* 2016;20(2):215–25.
- [31] Dajnowicz S, Johnston RC, Parks JM, Blakeley MP, Keen DA, Weiss KL, et al. Direct visualization of critical hydrogen atoms in a pyridoxal 5'-phosphate enzyme. *Nat Commun* 2017;8(1):955.
- [32] Dajnowicz S, Parks JM, Hu X, Johnston RC, Kovalevsky AY, Mueser TC. Hyperconjugation promotes catalysis in a pyridoxal 5'-phosphate-dependent enzyme. *ACS Catal* 2018;8:6733–7.
- [33] Tripathi SM, Ramachandran R. Direct evidence for a glutamate switch necessary for substrate recognition: crystal structures of lysine  $\epsilon$ -aminotransferase (Rv3290c) from *Mycobacterium tuberculosis* H37Rv. *J Mol Biol* 2006;362(5):877–86.
- [34] Schoenhofen IC, Lunin VV, Julien JP, Li Y, Ajamian E, Matte A, et al. Structural and functional characterization of PseC, an aminotransferase involved in the biosynthesis of pseudaminic acid, an essential flagellar modification in *Helicobacter pylori*. *J Biol Chem* 2006;281(13):8907–16.
- [35] Guan LJ, Ohtsuka J, Okai M, Miyakawa T, Mase T, Zhi Y, et al. A new target region for changing the substrate specificity of amine transaminases. *Sci Rep* 2015;5:10753.
- [36] Tachiki T, Tochikura T. Separation of L-leucine-pyruvate and L-leucine- $\alpha$ -ketoglutarate transaminases in *Acetobacter suboxydans* and identification of their reaction products. *Agric Biol Chem* 1973;37(6):1439–48.
- [37] Tachiki T, Tochikura T. Purification and characterization of L-leucine- $\alpha$ -ketoglutarate transaminases from *Acetobacter suboxydans*. *Agric Biol Chem* 1976;40(11):2187–92.
- [38] Yvon M, Chambellan E, Bolotin A, Roudot-Algaron F. Characterization and role of the branched-chain aminotransferase (BcaT) isolated from *Lactococcus lactis* subsp. *cremoris* NCD0 763. *Appl Environ Microbiol* 2000;66(2):571–7.
- [39] Norton JE, Sokatch JR. Purification and partial characterization of the branched chain amino acid transaminase of *Pseudomonas aeruginosa*. *Biochim Biophys Acta* 1970;206(2):261–9.
- [40] Stekhanova TN, Rakitin AL, Mardanov AV, Bezsdudnova EY, Popov VO. A novel highly thermostable branched-chain amino acid aminotransferase from the crenarchaeon *Vulcanisaeta moutnovskia*. *Enzyme Microb Technol* 2017;96:127–34.
- [41] Yonaha K, Toyama S, Kagamiyama H. Properties of the bound coenzyme and subunit structure of omega-amino acid:pyruvate aminotransferase. *J Biol Chem* 1983;258(4):2260–5.
- [42] Yoshikane Y, Yokochi N, Yamasaki M, Mizutani K, Ohnishi K, Mikami B, et al. Crystal structure of pyridoxamine-pyruvate aminotransferase from *Mesorhizobium loti* MAFF303099. *J Biol Chem* 2008;283(2):1120–7.
- [43] Xing RY, Whitman WB. Characterization of amino acid aminotransferase of *Methanococcus aeolicus*. *J Bacteriol* 1992;174(2):541–8.
- [44] Börner T, Rämisch S, Reddem ER, Bartsch S, Vogel A, Thunnissen AWH, et al. Explaining operational instability of amine transaminase: substrate-induced inactivation mechanism and influence of quaternary structure on enzyme-cofactor intermediate stability. *ACS Catal* 2017;7(2):1259–69.
- [45] Kumar S, Ma B, Tsai CJ, Sinha N, Nussinov R. Folding and binding cascades: dynamic landscapes and population shifts. *Protein Sci* 2000;9(1):9–10.
- [46] Goh CS, Milburn D, Gerstein M. Conformational changes associated with protein-protein interactions. *Curr Opin Struct Biol* 2004;14(1):104–9.
- [47] Tobi D, Bahar I. Structural changes involved in protein binding correlate with intrinsic motions of proteins in the unbound state. *Proc Natl Acad Sci U S A* 2005;102(52):18908–13.
- [48] Boehr DD, McElheny D, Dyson HJ, Wright PE. The dynamic energy landscape of dihydrofolate reductase catalysis. *Science* 2006;313(5793):1638–42.
- [49] Okazaki K, Takada S. Dynamic energy landscape view of coupled binding and protein conformational change: induced-fit versus population-shift mechanisms. *Proc Natl Acad Sci U S A* 2008;105(32):11182–7.
- [50] Włodarski T, Zagrobiec B. Conformational selection and induced fit mechanism underlie specificity in noncovalent interactions with ubiquitin. *Proc Natl Acad Sci U S A* 2009;106(46):19346–51.
- [51] Garbuzynskiy SO, Melnik BS, Lobanov MY, Finkelstein AV, Galzitskaya OV. Comparison of X-ray and NMR structures: is there a systematic difference in residue contacts between X-ray and NMR-resolved protein structures? *Proteins* 2005;60(1):139–47.
- [52] Sikic K, Tomic S, Carugo O. Systematic comparison of crystal and NMR protein structures deposited in the protein data bank. *Open Biochem J* 2010;4:83–95.
- [53] Montioli R, Zamparelli C, Voltattorni CB, Cellini B. Oligomeric state and thermal stability of apo- and holo-human ornithine  $\delta$ -aminotransferase. *Protein J* 2017;36(3):174–85.

- [54] Koshland DE. Application of a theory of enzyme specificity to protein synthesis. Proc Natl Acad Sci U S A 1958;44(2):98–104.
- [55] Ishijima J, Nakai T, Kawaguchi S, Hirotsu K, Kuramitsu S. Free energy requirement for domain movement of an enzyme. J Biol Chem 2000;275(25):18939–45.
- [56] Okamoto A, Higuchi T, Hirotsu K, Kuramitsu S, Kagamiyama H. X-ray crystallographic study of pyridoxal 5'-phosphate-type aspartate aminotransferase from *Escherichia coli* in open and closed form. J Biochem 1994;116(1):95–107.
- [57] Baker NA, Sept D, Joseph S, Holst MJ, McCammon JA. Electrostatics of nanosystems: application to microtubules and the ribosome. Proc Natl Acad Sci U S A 2001;98(18):10037–41.
- [58] Wade RC, Gabdoulline RR, Luty BA. Species dependence of enzyme-substrate encounter rates for triose phosphate isomerases. Proteins 1998;31(4):406–16.
- [59] Wade RC, Gabdoulline RR, Lüdemann SK, Lounnas V. Electrostatic steering and ionic tethering in enzyme-ligand binding: insights from simulations. Proc Natl Acad Sci U S A 1998;95(11):5942–9.
- [60] Tan RC, Truong TN, McCammon JA, Sussman JL. Acetylcholinesterase: electrostatic steering increases the rate of ligand binding. Biochemistry 1993;32(2):401–3.
- [61] Sharp K, Fine R, Honig B. Computer simulations of the diffusion of a substrate to an active site of an enzyme. Science 1987;236(4807):1460–3.
- [62] Getzoff ED, Cabelli DE, Fisher CL, Parge HE, Viezzoli MS, Banci L, et al. Faster superoxide dismutase mutants designed by enhancing electrostatic guidance. Nature 1992;358(6384):347–51.
- [63] Ripoll DR, Faerman Ch, Axelsen PH, Silman I, Sussman JL. An electrostatic mechanism for substrate guidance down the aromatic gorge of acetylcholinesterase. Proc Natl Acad Sci U S A 1993;90(11):5128–32.